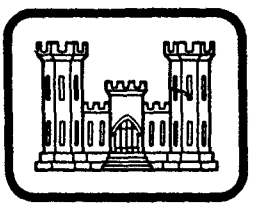

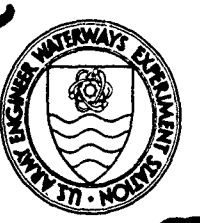

MISCELLANEOUS PAPER SL-81-3

12

ANALYSIS OF STEERABILITY OF TRACKED VEHICLES; THEORETICAL PREDICTIONS VERSUS FIELD MEASUREMENTS

by

George Y. Baladi and Behzad Rohani

Structures Laboratory
U. S. Army Engineer Waterways Experiment Station
P. O. Box 631, Vicksburg, Miss. 39180

March 1981
Final Report

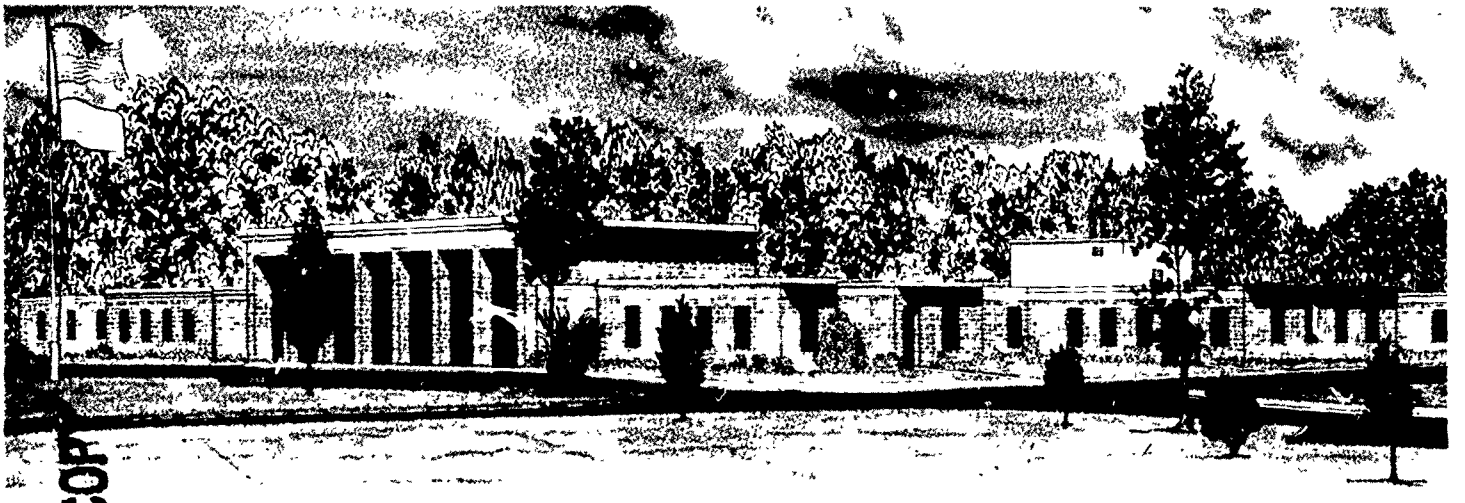

Prepared for Office, Chief of Engineers, U. S. Army
Washington, D. C. 20314

Under Project 4A161102AT22, Task CO, Work Unit 001

Monitored by Geotechnical Laboratory
U. S. Army Engineer Waterways Experiment Station
P. O. Box 631, Vicksburg, Miss. 39180

Destroy this report when no longer needed. Do not return it to the originator.

The findings in this report are not to be construed as an official Department of the Army position unless so designated by other authorized documents.

The contents of this report are not to be used for advertising, publication, or promotional purposes. Citation of trade names does not constitute an official endorsement or approval of the use of such commercial products.

Unclassified

SECURITY CLASSIFICATION OF THIS PAGE (When Data Entered)

REPORT DOCUMENTATION PAGE	READ INSTRUCTIONS BEFORE COMPLETING FORM
1. REPORT NUMBER: Miscellaneous Paper SL-81-3	2. GOVT ACCESSION NO.: AD-A098 777
3. RECIPIENT'S CATALOG NUMBER	
4. TITLE (and Subtitle): ANALYSIS OF STEERABILITY OF TRACKED VEHICLES: THEORETICAL PREDICTIONS VERSUS FIELD MEASUREMENTS	5. TYPE OF REPORT & PERIOD COVERED: Final Report; Oct 80 - Jan 81
6. PERFORMING ORG. REPORT NUMBER	
7. AUTHOR(s): George Y. Baladi, Behzad Rohani	8. CONTRACT OR GRANT NUMBER(s)
9. PERFORMING ORGANIZATION NAME AND ADDRESS: U. S. Army Engineer Waterways Experiment Station, Structures Laboratory, P. O. Box 631, Vicksburg, Miss. 39180	10. PROGRAM ELEMENT, PROJECT, TASK AREA & WORK UNIT NUMBERS: Project 4A161102AT22, Task CO, Work Unit 001
11. CONTROLLING OFFICE NAME AND ADDRESS: Office, Chief of Engineers, U. S. Army, Washington, D. C. 20314	12. REPORT DATE: March 1981
	13. NUMBER OF PAGES: 43
14. MONITORING AGENCY NAME & ADDRESS (If different from Controlling Office): U. S. Army Engineer Waterways Experiment Station, Geotechnical Laboratory, P. O. Box 631, Vicksburg, Miss. 39180	15. SECURITY CLASS. (of this report): Unclassified
	15a. DECLASSIFICATION/DOWNGRADING SCHEDULE

16. DISTRIBUTION STATEMENT (of this Report)

Approved for public release; distribution unlimited.

17. DISTRIBUTION STATEMENT (of the abstract entered in Block 20, if different from Report)

18. SUPPLEMENTARY NOTES

This paper was prepared for presentation at the Seventh International Congress of the International Society for Terrain-Vehicle Systems, 16-20 August 1981, Calgary, Canada.

19. KEY WORDS (Continue on reverse side if necessary and identify by block number)

AGIL (Computer program)	Steering
Computer programs	Terrain-vehicle interaction
Mathematical models	Tracked vehicles
Soil properties	Vehicle performance

20. ABSTRACT (Continue on reverse side if necessary and identify by block number)

A mathematical model has been developed for predicting the steering performance of high-mobility/agility tracked vehicles in environments ranging from very soft soils to hard surfaces such as rigid pavements. The tractive forces between the terrain and the vehicle track are simulated by a rheological model that accounts for nonlinear shear-stress/shear-deformation behavior, the effect of deformation rate on shearing resistance, and the effect of pressure on shear resistance and plastic yielding. The rheological model is coupled

(Continued)

DD FORM 1 JAN 73 1473 EDITION OF 1 NOV 65 IS OBSOLETE

Unclassified

SECURITY CLASSIFICATION OF THIS PAGE (When Data Entered)

20. ABSTRACT (Continued)

with the kinematics and the characteristics of the vehicle to develop the general equations governing the transient as well as the steady-state turning motion of a vehicle on a level, flat surface. A computer program, named AGIL, numerically integrates and solves these equations of motion in terms of the kinematics of the problem. The model is partially validated by comparing field measurements from a series of steering tests conducted in the vicinity of Vicksburg, Mississippi, with the corresponding model predictions.

PREFACE

This paper was prepared for presentation at the Seventh International Congress of the International Society for Terrain-Vehicle Systems, 16-20 August 1981, Calgary, Canada.

The investigation was conducted for the Office, Chief of Engineers, U. S. Army, by personnel of the Geomechanics Division (GD), Structures Laboratory (SL), U. S. Army Engineer Waterways Experiment Station (WES), as a part of Project 4A161102AT22, "Dynamic Soil-Track Interactions Governing High-Speed Combat Vehicle Performance."

This study was conducted by Drs. George Y. Baladi and Behzad Rohani during the period October 1980 - January 1981 under the general direction of Mr. Bryant Mather, Chief, SL; Dr. J. G. Jackson, Jr., Chief, GD; and Mr. C. J. Nuttall, Jr., Chief, Mobility Systems Division, Geotechnical Laboratory. The paper was written by Drs. Baladi and Rohani.

LTC David C. Girardot, Jr., CE, was Acting Commander of the WES during the investigation. Mr. F. R. Brown was Acting Director.

CONTENTS

ANALYSIS OF STEERABILITY OF TRACKED VEHICLES; THEORETICAL PREDICTIONS VERSUS FIELD MEASUREMENTS

PART I: INTRODUCTION

1. Development of high-mobility/agility tracked combat vehicles has received considerable attention recently because of the possibilities they offer for increased battlefield survivability through the avoidance, by high-speed and violent maneuver, of hits by high-velocity projectiles and missiles. In order to design and develop such vehicles rationally, it is necessary to have a quantitative understanding of the interrelationship between the terrain factors (such as soil type, soil shear strength and compressibility, etc.) and the vehicle's characteristics (weight, track length and width, location of center of gravity, velocity, etc.) during steering. To study such an interrelationship, it is necessary to construct idealized mathematical models of the terrain-vehicle interaction. The accuracy and range of application of such models must, of course, be determined from actual mobility experiments and obviously must depend on the degree of relevance of the idealized model as an approximation to the real behavior.

2. The basic concepts of the theory of terrain-vehicle interaction were developed by Bekker during the 1950's (Reference 1). By assuming various load distributions along the tracks, Bekker was able to develop several mathematical expressions relating the characteristics of the vehicle and the tractive effort of the terrain during steering. By considering the lateral and longitudinal coefficients of friction between the track and the ground, Hayashi (Reference 2) developed simple equations for practical analysis of steering of tracked vehicles. Hayashi's work, however, did not include the effect of the centrifugal forces on steering performance of the vehicle. Kitano and Jyorzaki (Reference 3) developed a more comprehensive model for uniform turning motion including the effects of centrifugal forces. This model, however, is based on the assumption that ground pressure is concentrated under each road wheel and the terrain-track interaction is simulated by Coulomb-type friction. The model given by Kitano and Jyorzaki was extended by Kitano and Kuma (Reference 4) to include nonuniform (transient) motion, but the basic elements of the terrain-track interaction part

of the model were retained. Baladi and Rohani (Reference 5) developed a model for uniform turning motion parallel to the development reported in Reference 3 insofar as the kinematics of the vehicle are concerned. In contrast to Reference 3, however, this model is based on a more comprehensive soil model. In the present paper, the terrain-vehicle model reported in Reference 5 is extended to include nonuniform (transient) motion. In addition, the soil model is modified to include a nonlinear failure envelope describing the shearing strength of the terrain material.

3. To demonstrate the application of the model, the steering performance of an armored personnel carrier has been predicted and correlated with full-scale test results.

PART II: SOIL MODEL

Strength Components

4. One of the most important properties of soil affecting trafficability is the in situ shear strength of the soil. The shear strength of earth materials varies greatly for different types of soil and is dependent on the confining pressure and time rate of loading (shearing). This dependence, however, is not the same for all soils and varies with respect to two fundamental strength properties of soil: the cohesive and the frictional properties. It has been found experimentally that the shear strength of purely cohesive soils (soils without frictional strength) is independent of the confining stress and is strongly affected by the time rate of shearing. On the other hand, in the case of purely frictional soil (soils without cohesive strength), the shear strength is found to be independent of time rate of loading and is strongly dependent on the confining pressure. In nature, most soils exhibit shearing resistance due to both the frictional and cohesive components. The cohesive and frictional components of strength are usually added together in order to obtain the total shear strength of the material; i.e.,

$$\tau_M = A - M \exp(-N\sigma) \tag{1}$$

where τ_M is the maximum shearing strength of the material, $C = A - M$ is the cohesive strength of the material corresponding to static loading (very slow rate of deformation), σ is normal stress, and N is a material constant. Equation 1 is shown graphically in Figure 1.

Effect of Rate of Deformation

5. As was pointed out previously, the cohesive strength of the material is dependent on the time rate of loading (shearing); i.e., the cohesive component of strength increases with increasing rate of loading. For the range of loading rates associated with the motion of tracked vehicles, the contribution to cohesive strength due to dynamic loading can be expressed as

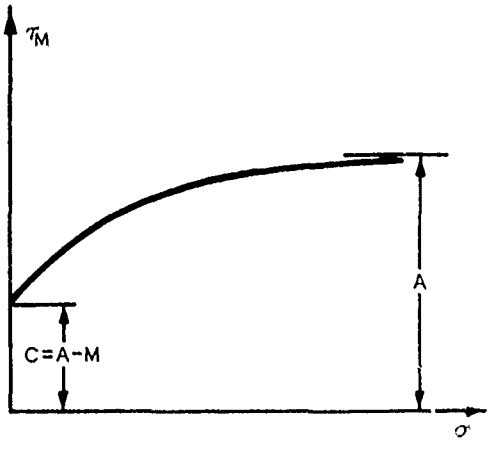

Figure 1. Propose failure relation for soil.

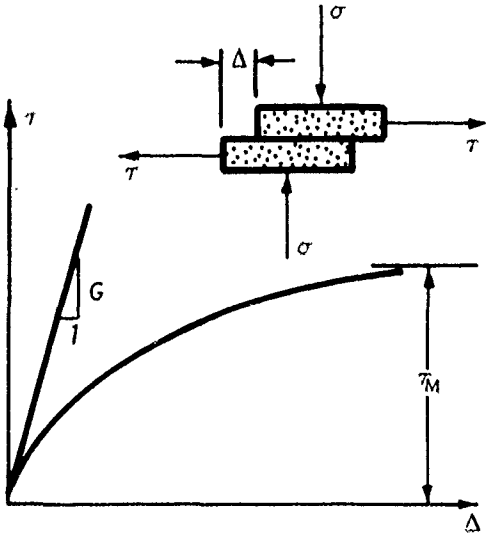

Figure 2. Proposed soil stress/deformation relation during shearing process.

$C_d[1 - \exp(-\Lambda\dot{\Delta})]$, where C_d and Λ are material constants, and $\dot{\Delta}$ is time rate of shearing deformation. In view of the above expression and Equation 1, the dynamic failure criterion takes the following form:

$$\tau_M = A + C_d[1 - \exp(-\Lambda\dot{\Delta})] - M \exp(-N\sigma) \tag{2}$$

Shear Stress-Shear Deformaton Relation

6. Prior to failure, the shear stress-shear deformation characteristics of a variety of soils can be expressed by the following mathematical expression (Reference 6):

$$\tau = \frac{G\,\tau_M\,\Delta}{\tau_M + G|\Delta|} \tag{3}$$

The behavior of Equation 3 is shown graphically in Figure 2. In Figure 2, τ denotes shearing stress, Δ is shearing deformation, and G is the initial shear stiffness coefficient. In view of Equation 2, the shear stress-shear deformation relation for soil (Equation 3) becomes

$$\tau = \frac{G[A + C_d - C_d \exp(-\Lambda\dot{\Delta}) - M \exp(-N\sigma)]\Delta}{G|\Delta| + A + C_d - C_d \exp(-\Lambda\dot{\Delta}) - M \exp(-N\sigma)} \tag{4}$$

For purely cohesive soils, $N = 0$ and τ is only a function of Δ and $\dot{\Delta}$. For granular material, $M = A$ and C_d is zero, and τ is a function of Δ and σ . For mixed soils exhibiting shearing resistance due to both frictional and cohesive components, τ is dependent on Δ , $\dot{\Delta}$, and σ . An appropriate test for determining the numerical values of the six material constants in Equation 4 is an in situ direct shear test. A field direct shear device has been developed at WES for this purpose. A description of this device and the method of analysis of the data obtained from the direct shear test are documented in Appendix C of Reference 7. In the following section, the equations of motions for a track-laying vehicle during steering are developed using the proposed soil model (Equation 4) in conjunction with track slippage, centrifugal forces, and vehicle characteristics.

PART III: DERIVATION OF TERRAIN-VEHICLE MODEL

Boundary Conditions

7. The geometry of the vehicle and the boundary conditions of the proposed model are shown schematically in Figure 3. The XYZ coordinates are the local coordinate system of which X is always the longitudinal axis of the vehicle and Y is a transverse axis parallel to the ground. These axes intersect at the center of geometry of the vehicle O. The Z axis is a vertical axis passing through the origin O. The center of gravity of the vehicle (CG) lies on the X axis and is displaced by a distance C_X from the origin. The numerical value of C_X is assumed to be positive if CG is displaced forward from the center of geometry of the vehicle. The XY coordinates of the instantaneous center of rotation (ICR) are $P + C_X$ and $\tilde{R}$, respectively, where P is the offset. The center of rotation and the radius of the trajectory of the CG are, respectively, CR and R_o. The height of the center of gravity measured from ground surface is denoted by H. The lengths of the track-ground contact, the track width, and the tread of the tracks are L, D, and B, respectively. As shown in Figure 3, the components of the inertial forces F_C in X and Y directions are, respectively, F_{CX} and F_{CY}. The weight of the vehicle is W.

Stress Distribution Along the Tracks

8. Two types of stress (i.e., normal and shear stresses) exist along the track. As indicated in Figure 3, the normal stresses under the outer and inner tracks are denoted by $R_1(X)$ and $R_2(X)$, respectively. The components of the shear stress in X and Y directions are, respectively, $T_1(X)$ and $Q_1(X)$ for the outer track, and $T_2(X)$ and $Q_2(X)$ for the inner track. These stresses are dependent on the terrain type, vehicle configuration, and speed and turning radius of the vehicle.

9. The magnitude of normal stresses $R_1(X)$ and $R_2(X)$ can be determined in terms of the components of the inertial force, the track tensions, and the characteristics of the vehicle by considering the balance of vertical stresses and their moments in Figure 3.* Thus:

---

* For sake of brevity, the effect of track tension is not included in this paper and was "turned off" in the computer program AGIL. The reader is referred to Reference 7 for a complete analysis of track tension and its effect on steering performance of tracked vehicles.

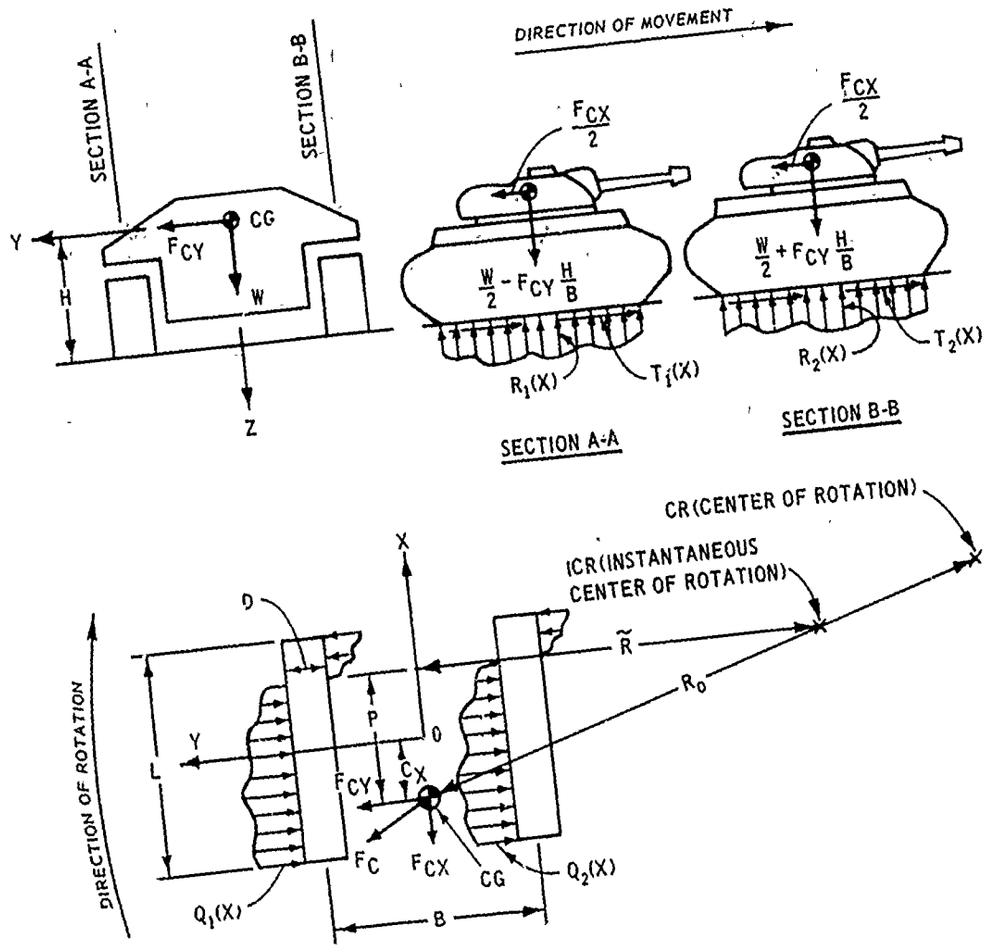

Figure 3. Geometry and boundary conditions of the terrain-vehicle model.

$$R_1(x) = \frac{W}{dL^2}\left(\frac{1}{2} + 6xc_X - \frac{h}{b}\frac{F_{CX}}{W} - 6hx\frac{F_{CX}}{W}\right) \tag{5}$$

$$R_2(x) = \frac{W}{dL^2}\left(\frac{1}{2} + 6xc_X + \frac{h}{b}\frac{F_{CY}}{W} - 6hx\frac{F_{CX}}{W}\right) \tag{6}$$

where $h = H/L$, $b = B/L$, $d = D/L$, $c_X = C_X/L$, $x = X/L$, $y = Y/L$, and $z = Z/L$.

10. The components of the shear stress in the X and Y directions along both the outer and inner tracks can be obtained by combining Equations 4, 5, and 6.* Thus (it is noted that R_1 and R_2 replace the normal stress σ in Equation 4):

$$T_i(x) = \frac{W}{L^2}\mu\delta_i\left\{\frac{da+dc_d-dc_d\exp(-\lambda\dot{\delta}_i)-m\exp[-nr_i(x)]}{\mu|\dot{\delta}_i|d+da+dc_d-dc_d\exp(-\lambda\dot{\delta}_i)-m\exp[-nr_i(x)]}\right\}\cos\gamma_i \tag{7}$$

$$Q_i(x) = \frac{W}{L^2}\mu\delta_i\left\{\frac{da+dc_d-dc_d\exp(-\lambda\dot{\delta}_i)-m\exp[-nr_i(x)]}{\mu|\dot{\delta}_i|d+da+dc_d-dc_d\exp(-\lambda\dot{\delta}_i)-m\exp[-nr_i(x)]}\right\}\sin\gamma_i \tag{8}$$

where $i = 1,2$; $r_i(x) = dL^2R_i(x)/W$; $\delta_i = \Delta_i/L$; $\dot{\delta}_i = \dot{\Delta}_i/L$; $\mu = GL^3/W$; $\lambda = \Lambda L$; $a = AL^2/W$; $m = ML^2/W$; $n = NW/L^2$; and $c_d = C_dL^2/W$. The variables γ_1 and γ_2 , in Equations 7 and 8, are the slip angles and can be written as

$$\gamma_1 = \tan^{-1}\frac{X - P - C_X}{C_1} = \tan^{-1}\frac{x - p - c_X}{\xi_1}$$

$$\gamma_2 = \tan^{-1}\frac{X - P - C_X}{C_2} = \tan^{-1}\frac{x - p - c_X}{\xi_2} \tag{9}$$

where $\xi_1 = C_1/L$, $\xi_2 = C_2/L$, and $p = P/L$. The parameter C_1 is the distance between the instantaneous center of rotation of the outer track and its axis of symmetry, and C_2 is the distance between the instantaneous center of rotation of the inner track and its axis of symmetry.

---

* To account for the effect of the size of the shear box on the shear stiffness G , the measured value of G is normalized in AGIL by multiplying it by $4/L$ (the length of the shear box = 4 in.).

11. In order to use Equations 7 through 9, the track slip velocities and displacements (i.e., $\dot{\Delta}_1$, Δ_1, $\dot{\Delta}_2$, and Δ_2) and the inertial forces, F_{CX} and F_{CY}, have to be determined.

Kinematics of the Vehicle

12. A tracked vehicle in transient motion is shown schematically in Figure 4. The XYZ coordinates are the local coordinate systems that are fixed with respect to the moving vehicle (also see Figure 3). The origin O of this coordinate system stays, for all time, at a distance C_X from the center of gravity of the vehicle. The $\Psi\Phi$ coordinate system is fixed on level ground, and its origin coincides with the center of gravity at time zero. The vehicle can maneuver on the $\Psi\Phi$ plane and the displacements of the center of gravity of the vehicle from this reference frame are $\Psi(t)$ and $\Phi(t)$.

13. The velocities v_X and v_Y (relative to the origin of the $\Psi\Phi$ coordinate system) as well as the velocities v_Ψ and v_Φ are related to the instantaneous velocity v of the CG by

$$v = \sqrt{v_X^2 + v_Y^2} = \sqrt{v_\Psi^2 + v_\Phi^2} \tag{10}$$

The side-slip angle α, which is the angle between the velocity vector v and the longitudinal X axis of the vehicle, is related to the velocities v_X and v_Y as

$$\alpha = \tan^{-1}\frac{v_Y}{v_X}, \quad \frac{d\alpha}{dt} = \left(v_X\frac{dv_Y}{dt} - v_Y\frac{dv_X}{dt}\right)\Big/ v^2 \tag{11}$$

The yaw angle ω and the directional angle Θ are related to α as

$$\Theta = \omega - \alpha, \quad \frac{d\Theta}{dt} = \frac{d\omega}{dt} - \frac{d\alpha}{dt} \tag{12}$$

Substitution of Equation 11 into Equation 12 leads to

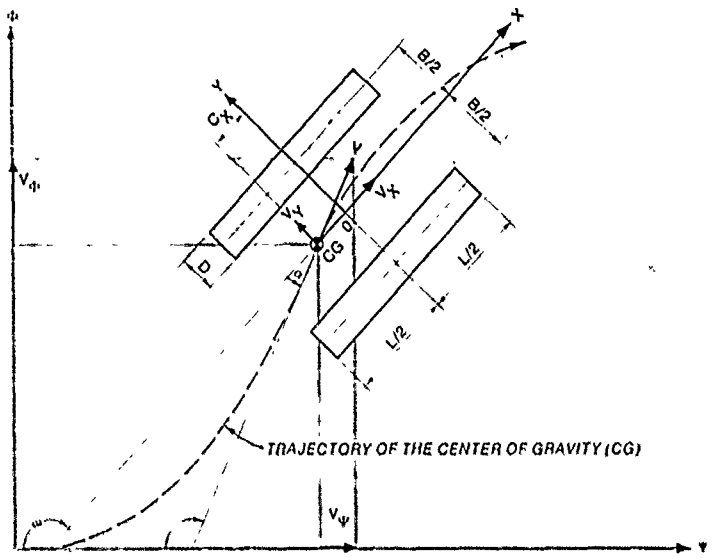

Figure 4. Tracked vehicle in transient motion.

$$\frac{d\Theta}{dt} = \frac{d\omega}{dt} - \left(v_X \frac{dv_Y}{dt} - v_Y \frac{dv_X}{dt}\right) \Big/ v^2 \tag{13}$$

14. The radius of curvature of the trajectory of the center of gravity (i.e., the distance between CR and CG, Figure 3) is

$$R_o = v \Big/ \frac{d\Theta}{dt} = \frac{v^3}{v^2 \frac{d\omega}{dt} - v_X \frac{dv_Y}{dt} + v_Y \frac{dv_X}{dt}} \tag{14}$$

The coordinates of the trajectory of the center of gravity of the vehicle can be written as

$$\left.\begin{aligned} \Psi(t) &= -\int_0^t v \cos \Theta \, dt \\ \Phi(t) &= \int_0^t v \sin \Theta \, dt \end{aligned}\right\} \tag{15}$$

15. The coordinates of the instantaneous center of rotation (ICR) of the hull in the XY systems (X_I , Y_I) and the instantaneous radius of curvature are (Figure 3)

$$\left.\begin{aligned} X_I &= P + C_X = v_Y \Big/ \frac{d\omega}{dt} + C_X \\ Y_I &= \tilde{R} = v_X \frac{d\omega}{dt} \\ R_I &= \sqrt{\tilde{R}^2 + P^2} \end{aligned}\right\} \tag{16}$$

Track Slip Velocity and Displacement

16. Assume that v_{s1} ($v_{s1} = \dot{\Delta}_1$) and v_{s2} ($v_{s2} = \dot{\Delta}_2$) are the slip velocities of geometrically similar points of the outer track and the inner track, respectively. The X and Y components of these velocities can be shown to be

$$\left.\begin{aligned} v_{sX1} &= C_1 \frac{d\omega}{dt} = \xi_1 L \frac{d\omega}{dt} \\ v_{sY1} &= (X - P - C_X) \frac{d\omega}{dt} = L(x - c_X) \frac{d\omega}{dt} - v_Y \end{aligned}\right\} \text{ For the outer track} \qquad (17)$$

$$\left.\begin{aligned} v_{sX2} &= C_2 \frac{d\omega}{dt} = \xi_2 L \frac{d\omega}{dt} \\ v_{sY2} &= v_{sY1} \end{aligned}\right\} \text{ For the inner track} \qquad (18)$$

The angular velocity $d\omega/dt$ and $\tilde{R}$ can be written as

$$\left.\begin{aligned} \frac{d\omega}{dt} &= \frac{1}{bL} (v_{X1} - v_{sX1} - v_{X2} + v_{sX2}) \\ \tilde{R} &= \frac{1}{2\frac{d\omega}{dt}} (v_{X1} - v_{sX1} + v_{X2} - v_{sX2}) \end{aligned}\right\} \qquad (19)$$

where v_{X1} = the velocity of the outer track relative to the hull

v_{X2} = the velocity of the inner track relative to the hull

The ratio of v_{X1} and v_{X2} is defined as the steering ratio ε. Thus,

$$\varepsilon = v_{X1}/v_{X2} \qquad (20)$$

Substitution of Equations 16 and 20 into Equation 19 leads to

$$v_{sX1} = \varepsilon v_{X2} - \left(v_X + \frac{bL}{2} \frac{d\omega}{dt}\right) \quad \text{For the outer track} \qquad (21)$$

$$v_{sX2} = v_{X2} - \left(v_X - \frac{bL}{2} \frac{d\omega}{dt}\right) \quad \text{For the inner track} \qquad (22)$$

Comparison between Equations 21 and 22 and Equations 17 and 18 results in

$$\xi_1 = \left(\epsilon v_{X2} - v_X\right)\Big/\left(L\,\frac{d\omega}{dt}\right) - \frac{b}{2} \tag{23}$$

$$\xi_2 = \left(v_{X2} - v_X\right)\Big/\left(L\,\frac{d\omega}{dt}\right) + \frac{b}{2} \tag{24}$$

The slip velocities and displacements of the outer and inner tracks can be obtained from Equations 17, 18, 21, and 22. Thus,

$$\frac{v_{s1}}{\sqrt{Lg}} = \sqrt{\frac{L}{g}}\,\frac{d\omega}{dt}\sqrt{\xi_1^2 + \left[\left(x - c_X\right) - \frac{v_Y}{L\,\frac{d\omega}{dt}}\right]^2} \tag{25}$$

$$\frac{v_{s2}}{\sqrt{Lg}} = \sqrt{\frac{L}{g}}\,\frac{d\omega}{dt}\sqrt{\xi_2^2 + \left[\left(x - c_X\right) - \frac{v_Y}{L\,\frac{d\omega}{dt}}\right]^2} \tag{26}$$

$$\frac{\Delta_1}{L} = \int_0^{t_1} \frac{v_{s1}}{L}\,dt + \frac{\Delta_{I1}}{L}\,,\quad \frac{\Delta_2}{L} = \int_0^{t_2} \frac{v_{s2}}{L}\,dt + \frac{\Delta_{I2}}{L} \tag{27}$$

where $t_1 = (L/2 - X)/v_{X1}$

$t_2 = (L/2 - X)/v_{X2}$

Δ_{I1} = initial displacement of the outer track

Δ_{I2} = initial displacement of the inner track

The balance of forces and moments dictates that these initial displacements be numerically equal to $L\delta$ (δ is the coefficient of rolling resistance which must be measured experimentally or calculated from empirical relations such as those given in Reference 8 for each soil type and each vehicle).

Inertial Forces

17. The X and Y components of the inertial force can be shown to be (Reference 7)

$$F_{CX} = \frac{W}{g}\left(\frac{dv_X}{dt} + v_Y \frac{d\omega}{dt}\right), \quad F_{CY} = \frac{W}{g}\left(\frac{dv_Y}{dt} - v_X \frac{d\omega}{dt}\right) \tag{28}$$

The Rolling Resistance

18. The rolling resistance is a function of terrain type, vehicle speed, track condition, etc. Therefore, rolling resistance should be measured for every specific condition. In this formulation, however, the rolling resistance is assumed to be proportional to normal load. Thus,

$$R_s = \frac{W}{dL^2} \delta \int_{-\frac{1}{2}}^{\frac{1}{2}} [r_1(x) + r_2(x)]dx \tag{29}$$

Equations of Motion

19. Steerability and stability of tracked vehicles depend on the dynamic balance between all forces and moments applied on the vehicle. According to Figure 4, the following three equations govern the motion of the vehicle:

$$\int_{-\frac{1}{2}}^{\frac{1}{2}} [t_1(x) + t_2(x)]\, dx - \delta \int_{-\frac{1}{2}}^{\frac{1}{2}} [r_1(x) + r_2(x)]\, dx = f_{CX} \tag{30}$$

$$\int_{-\frac{1}{2}}^{\frac{1}{2}} [q_1(x) + q_2(x)]\, dx = f_{CY} \tag{31}$$

$$\int_{-\frac{1}{2}}^{\frac{1}{2}} [q_1(x) + q_2(x)]\ (x - c_X)\ dx + \frac{b}{2}\int_{-\frac{1}{2}}^{\frac{1}{2}} [t_1(x) - t_2(x)]dx$$

$$+ \frac{b}{2}\int_{-\frac{1}{2}}^{\frac{1}{2}} [r_2(x) - r_1(x)]dx = \frac{I_z}{LW}\frac{d^2\omega}{dt^2} \qquad (32)$$

where $t_1(x) = dL^2\ T_1(x)/W$, $t_2(x) = dL^2\ T_2(x)/W$, $q_1(x) = dL^2\ Q_1(x)/W$,

$q_2(x) = dL^2\ Q_2(x)/W$, $f_{CX} = F_{CX}/W$, and $f_{CY} = F_{CY}/W$

and I_z = mass moment of inertia about an axis passing through the center of gravity of the vehicle and parallel to the Z axis (Figure 3). Equations 30 through 32 with the aid of Equations 7 through 29 constitute three equations that involve three unknowns. The three unknowns are either v_X , v_Y , and $d\omega/dt$ or ξ_1 , ξ_2 , and p . In order to obtain a complete solution for either of the two sets of unknowns, one of the following driving conditions must be specified: (a) time history of the steering ratio $\varepsilon(t)$ and the initial speed of the vehicle, (b) time history of the velocity of the individual tracks $v_{X1}(t)$ and $v_{X2}(t)$ and the initial speed of the vehicle, (c) time history of the velocity of the vehicle $v(t)$ and the trajectory of motion, (d) time history of the velocity of the vehicle and a constant value of steering ratio ε , or (e) the trajectory of motion and a determination of the maximum velocity-time history at which the vehicle can traverse the specified trajectory. A computer program called AGIL was developed to solve Equations 30 through 32 using Newton's iteration technique. In addition, this computer program has the capability of calculating the total power requirements (PT) as well as the power required at each sprocket (Reference 7).

PART IV: CORRELATION OF THEORETICAL PREDICTIONS WITH TEST DATA

20. In order to determine the accuracy and range of application of the terrain-vehicle model a series of slalom and circular turn tests was conducted in several areas in the vicinity of Vicksburg, Mississippi. The results of these tests are presently being analyzed for correlation and comparison with the model predictions. Data from five turn tests (test series 107 through 111), however, have been reduced and are available for correlation analysis. These data offer the first opportunity to evaluate the accuracy of the terrain-vehicle model. A brief description of the test conditions for this series of tests and the analysis of the data and comparison with the model predictions are presented in the subsequent sections.

Experimental Program

21. Test series 107 through 111 was conducted in an area termed as New Ground Area, located north of Redwood, Mississippi. The area is barren and unplowed. The soil at this area is a soft plastic clay classified as CH according to the Unified Soil Classification System.* Each test involved the steering of the vehicle in a circular path by first accelerating the vehicle to a maximum speed (controlled by either the available power or the actual physical stability of the vehicle) and then continue turning with a more or less constant speed. The tracked vehicle used for these experiments is an armored personnel vehicle with the characteristics given in Table 1. The actual data collected during each test consisted of time histories of (a) the inner and outer track velocities, (b) the speed of the vehicle, (c) the turning radius, and (d) the power requirement. The lateral acceleration of the vehicle was then calculated from items b and c above. In addition to the above data, numerous slow and fast in situ direct shear tests were conducted at each test site in order to characterize the soil in terms of the soil parameters given in Equations 1 through 4. Table 2 summarizes the soil parameters for the New Ground Area. Also shown in Table 2 is the coefficient of rolling resistance for the vehicle which was obtained experimentally (through torque measurements for straightforward motion) at the site.

---

* The Unified Soil Classification System is described in Reference 9.

Table 1

Characteristics of Vehicle Used for Turn Tests

Weight (W)	=	18,000 lb
Track Length (L)	=	105 in.
Track Width (D)	=	15 in.
Tread (B)	=	90 in.
Height of the center of gravity (H)	=	35.7 in.
Moment of inertia (I_z)	=	92,000 lb-in.-sec^2
Location of the center of gravity measured from the geometrical center of the vehicle (C_x)	=	0

Table 2

Summary of the Soil Parameters for the New Ground Area

Initial shear stiffness coefficient (G)	=	200 psi/in.
Cohesive strength of the material corresponding to static loading (C = A - M)	=	0.94 psi
Static failure envelope (Equation 1) parameter (A)	=	5.00 psi
Static failure envelope (Equation 1) parameter (M)	=	4.06 psi
Static failure envelope (Equation 1) parameter (N)	=	0.22 1/psi
Dynamic failure envelope (Equation 2) parameter (C_d)	=	0.61 psi
Dynamic failure envelope (Equation 2) parameter (Λ)	=	3.68 sec/in.
Coefficient of rolling resistance (f)	=	0.2
WES cone index (CI) for 0- to 6-in. depth	=	30 psi
WES cone index (CI) for 6- to 12-in. depth	=	65 psi

The soil parameters A, M, and N in Table 2 were determined by fitting Equation 1 to the experimental static failure envelope of the soil (from slow tests). The initial shear stiffness modulus G was then determined by fitting Equations 1 and 3 to the experimental shear stress-shear deformation curves from slow tests. Finally the parameters C_d and Λ were obtained by fitting Equations 2 and 4 to the experimental failure envelope and shear stress-shear deformation curves from fast tests. The representative failure envelope obtained from experimental static data and the corresponding analytical curve (Equation 1) are shown in Figure 5. It is observed from Figure 5 that the agreement between the two curves is excellent. Typical experimental and the corresponding analytical static and dynamic shearing stress-shearing deformation curves for the clay soil from the New Ground Area are shown in Figure 6. Again, the experimental results and the model simulations are in close agreement.

Theoretical Predictions

22. The purpose of the circular turn tests was to create a condition of steady-state motion for the vehicle to evaluate the accuracy of the model for this simple mode of motion. Unfortunately, due to factors such as surface roughness, inhomogeneity of surface materials, and the fact that the ground is not an ideally flat, level surface, it is not possible to maintain the vehicle in a perfect steady-state mode of motion. These factors adversely affect the ability of the driver to steer the vehicle at a constant radius with a constant velocity. Therefore, the motion of the vehicle during the entire test event cannot be considered as steady-state motion. For this reason, for each test a time window was selected where the motion of the vehicle could be reasonably approximated as steady state. The time windows and the corresponding test data consisting of the steering ratio ϵ, vehicle velocity v, turning radius R_o, lateral acceleration $v^2/R_o g$ and total power PT are given in Table 3 for all the tests. The computer program AGIL was used to simulate these steady-state test conditions using the vehicle characteristics and the soil parameters from Tables 1 and 2, respectively. Comparisons of the model predictions with experimental data are presented in Figures 7 through 12 for turning radius versus steering ratio, inner track velocity versus turning radius, outer track velocity

Table 3

Steady-State Time Windows and Corresponding Test Data

Test No.	Time sec		Steering Ratio ε	Vehicle Speed v, mph	Turning Radius R_o, ft	Lateral Acceleration $v^2/R_o g$	Power PT, HP
107	60	66	1.08	24.88	155.77	0.265	210
108	81	84	1.29	14.93	63.69	0.234	199
109	37	42	1.12	15.73	103.86	0.16	177
	68	71	1.10	18.22	121.26	0.18	184
110	55	59	1.26	16.08	83.40	0.21	200
111	48	51	1.57	11.79	33.74	0.275	211

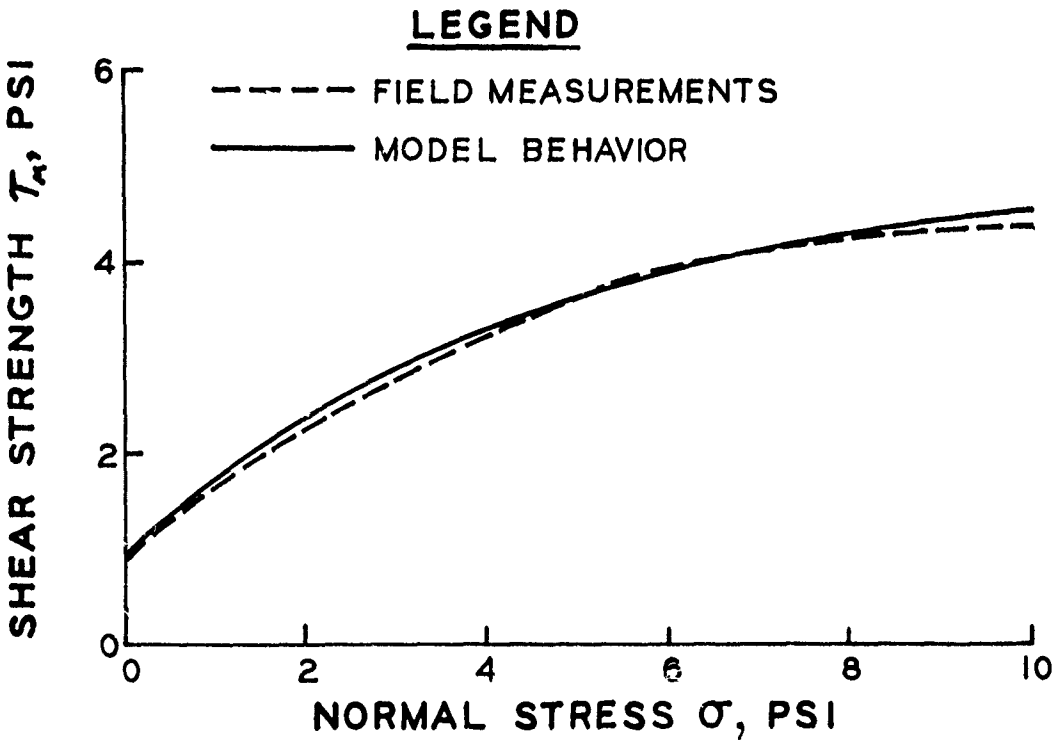

Figure 5. Comparison of experimntal static failure envelope with model behavior for clay soil from New Ground Area

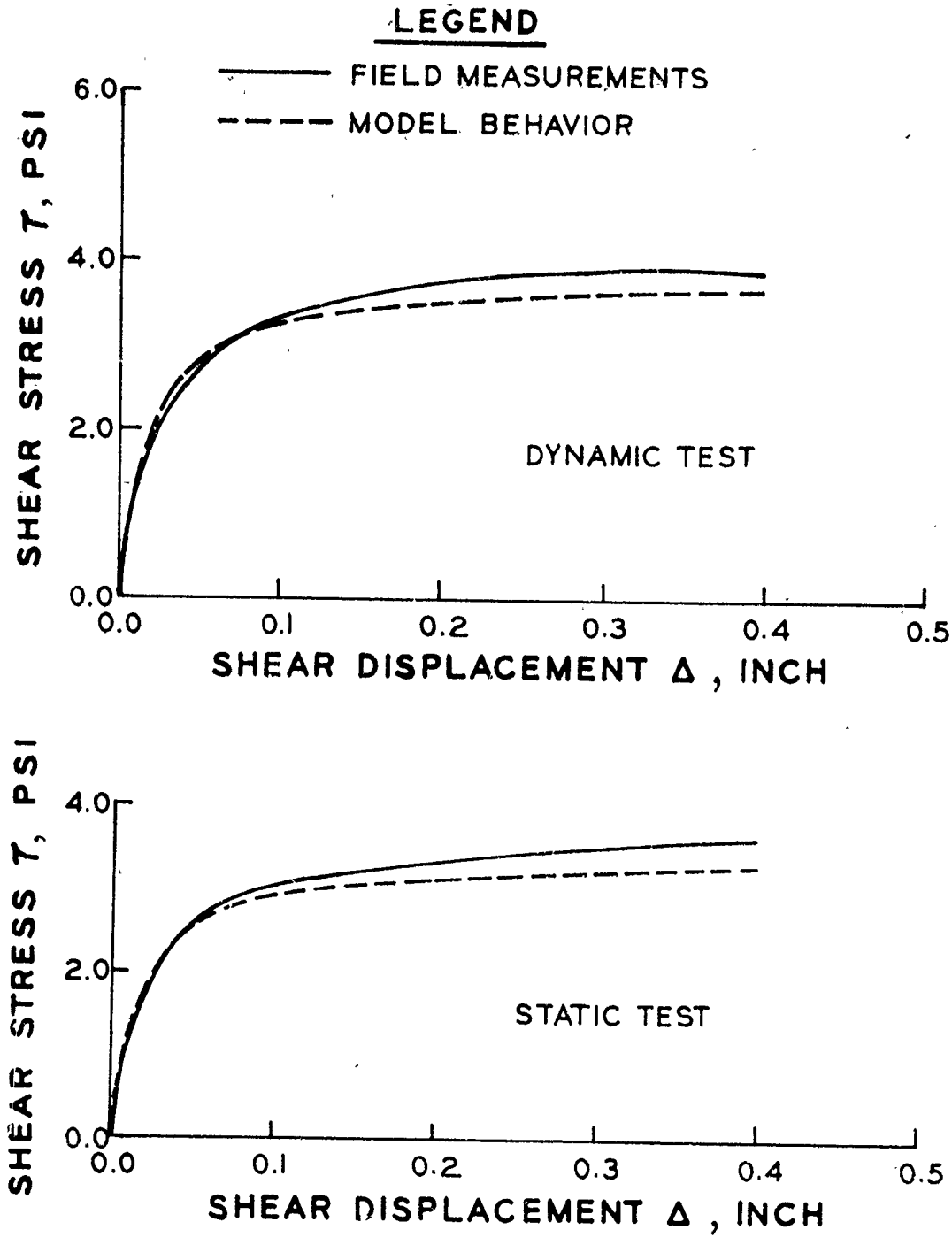

Figure 6. Comparison of experimental shearing stress-shearing displacement relation with model behavior (σ = 4.14 psi) for clay soil from New Ground Area

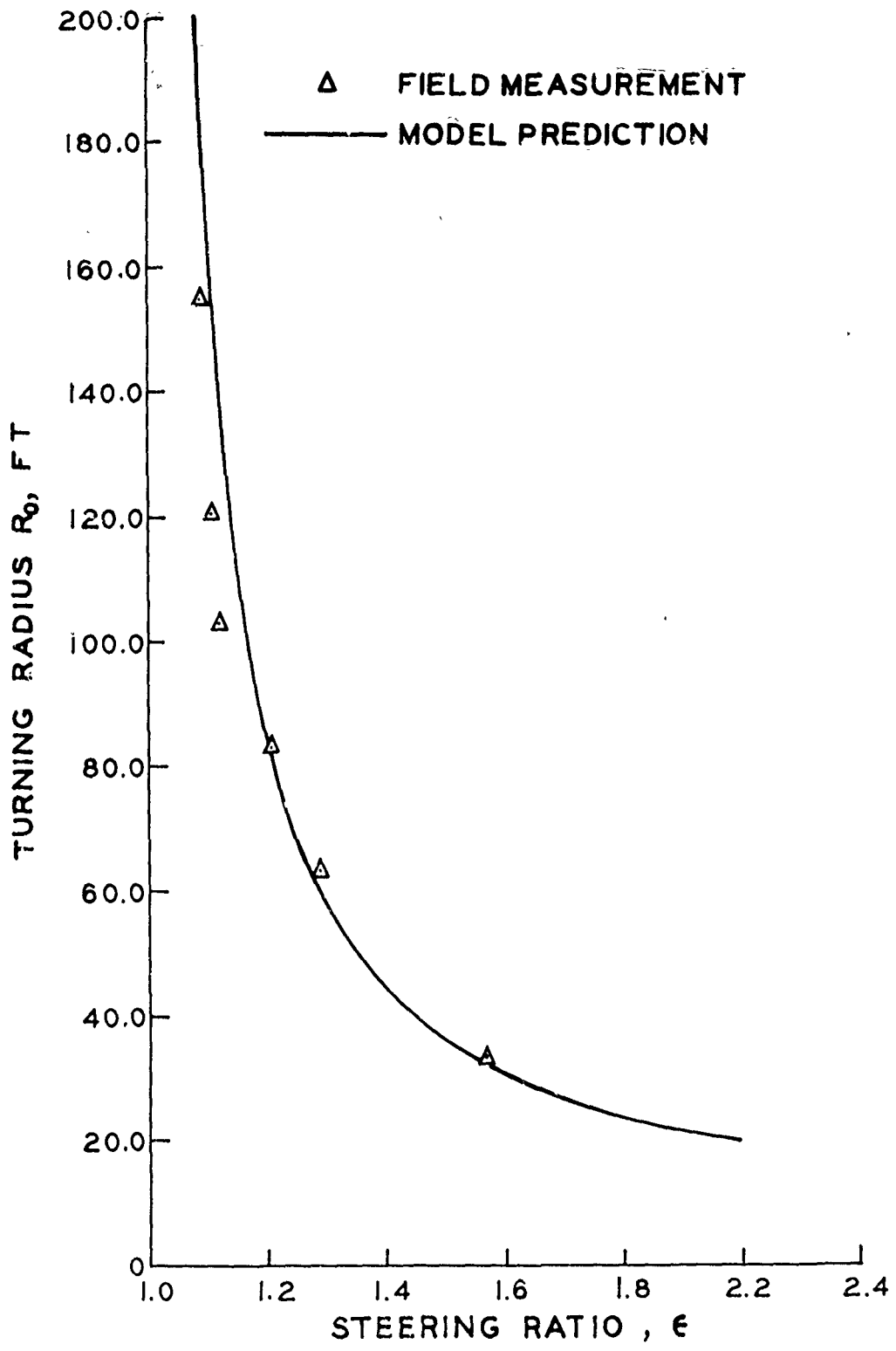

Figure 7. Turning radius versus steering ratio for test series 107-111; comparison of model predictions with experimental data

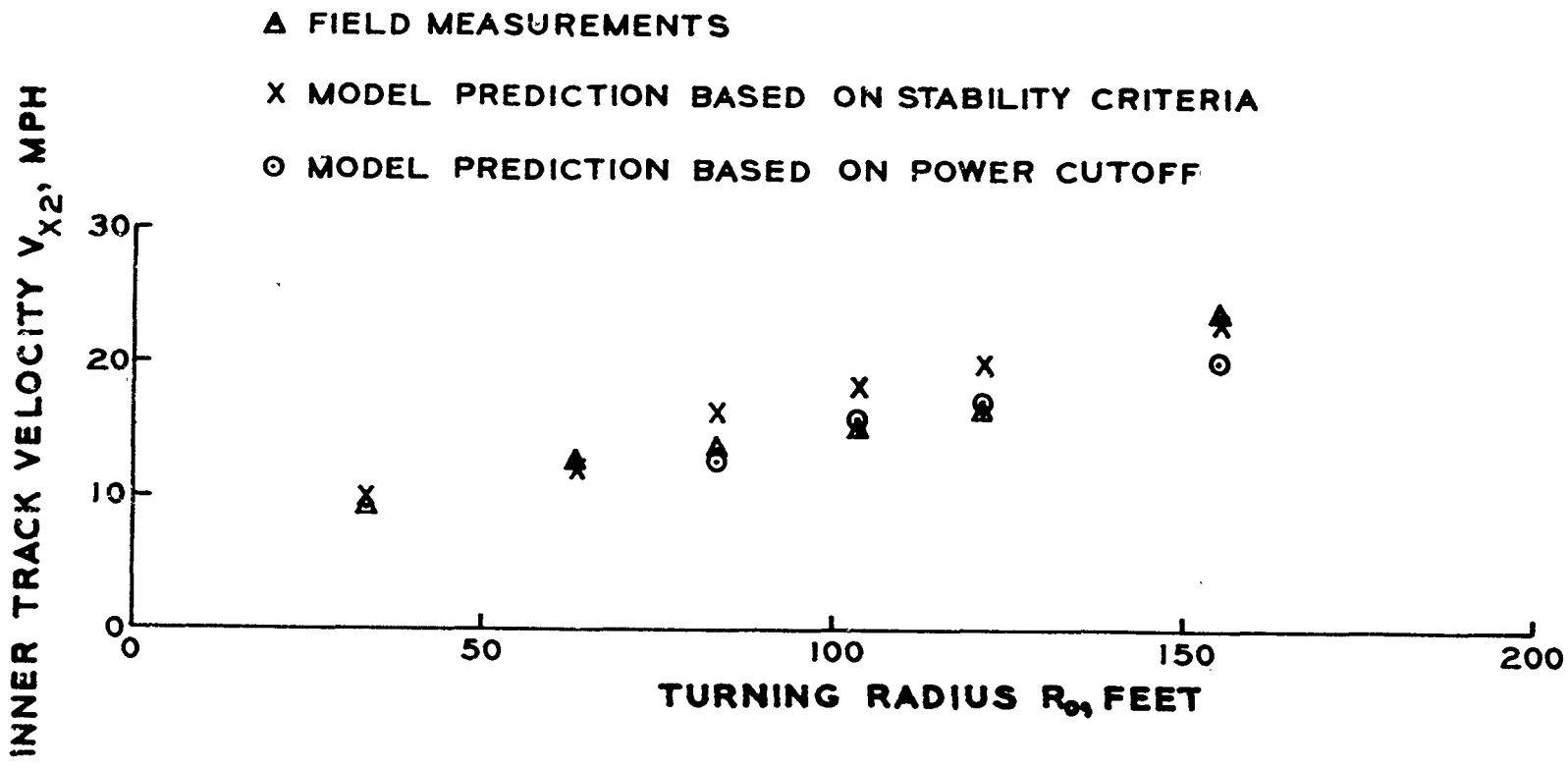

Figure 8. Inner track velocity versus turning radius for test series 107-111; comparison of model predictions with experimental data (for tests at radii of 33.74 and 63.69 ft, stability criteria govern the speed of the vehicle)

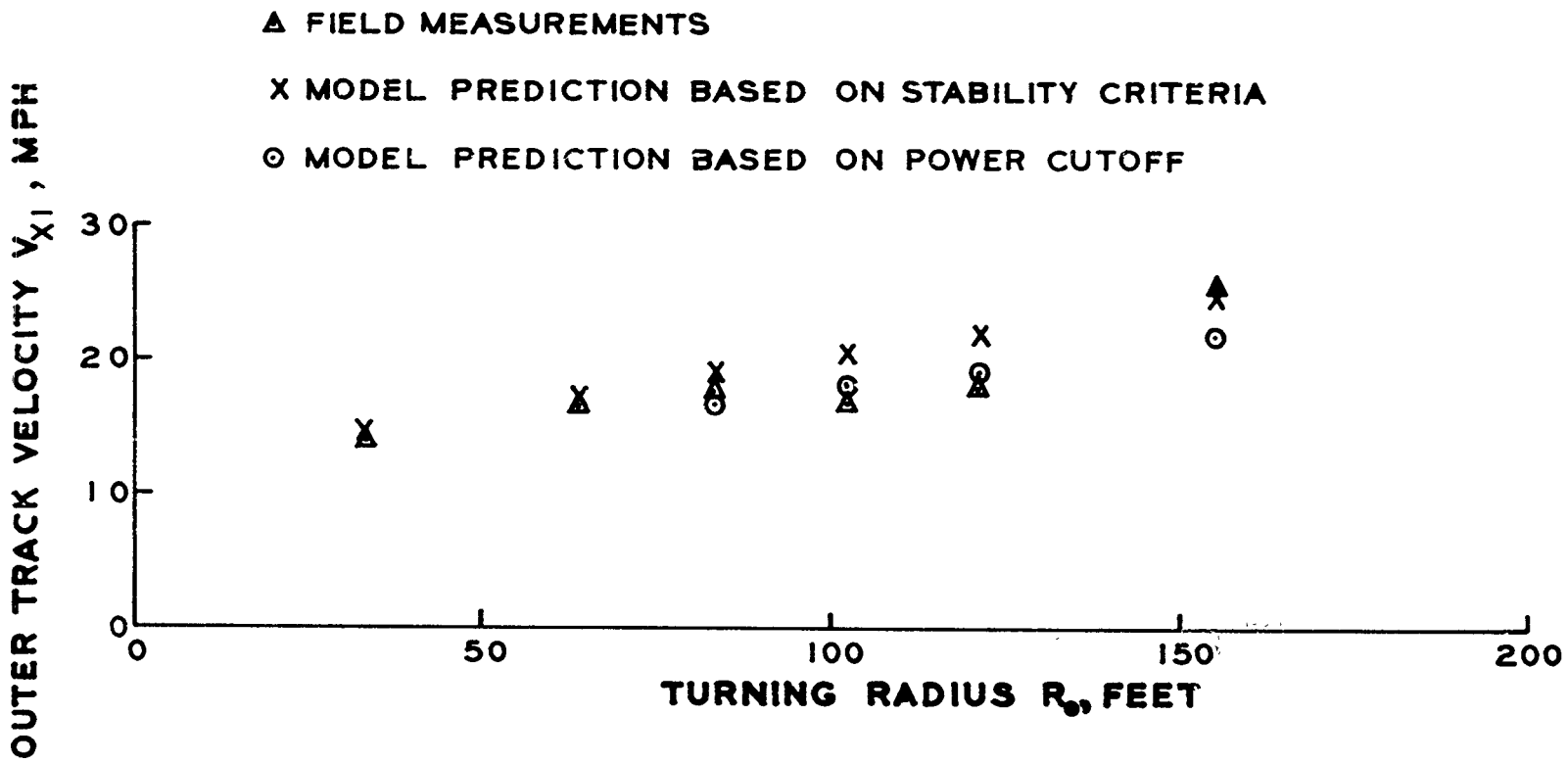

Figure 9. Outer track velocity versus turning radius for test series 107-111; comparison of model predictions with experimental data

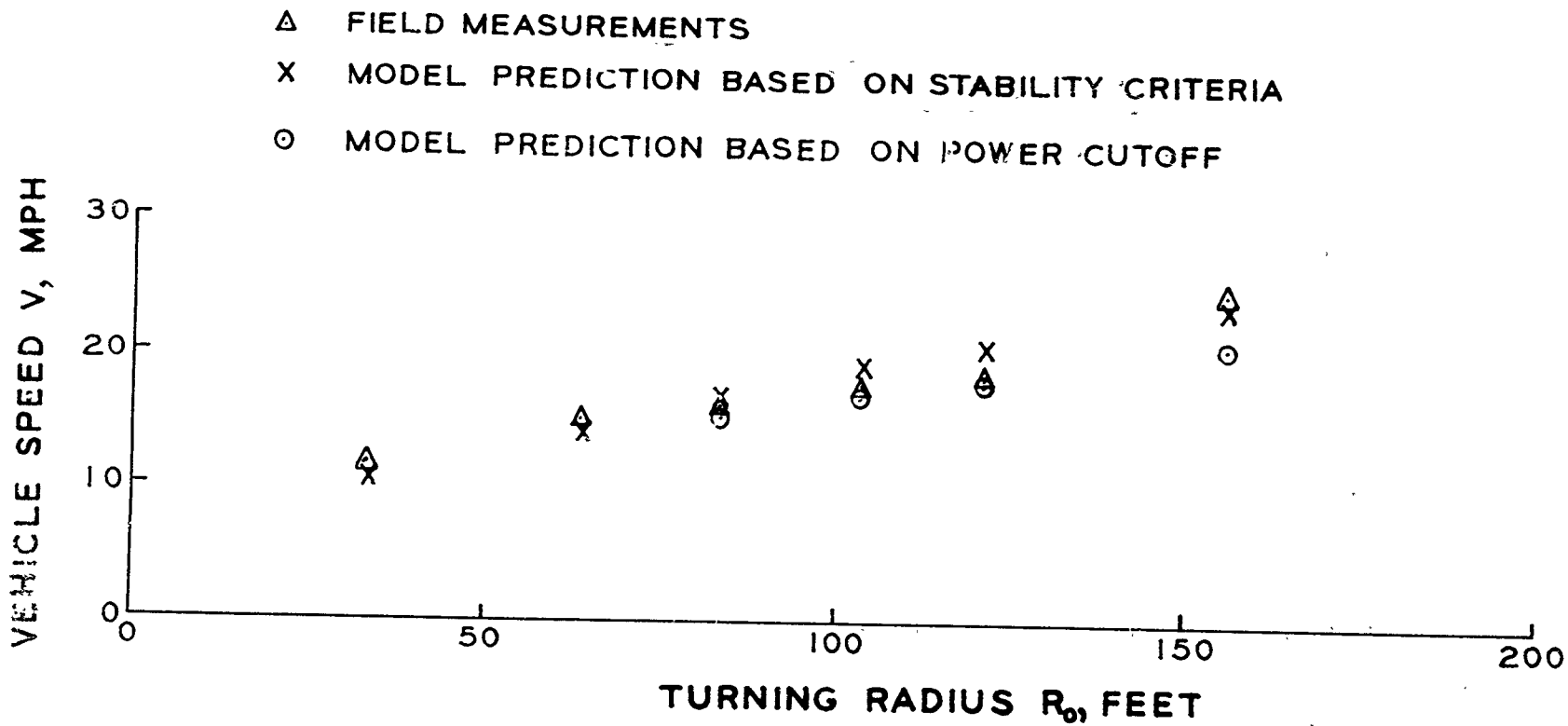

Figure 10. Vehicle speed versus turning radius for test series 107-111; comparison of model predictions with experimental data

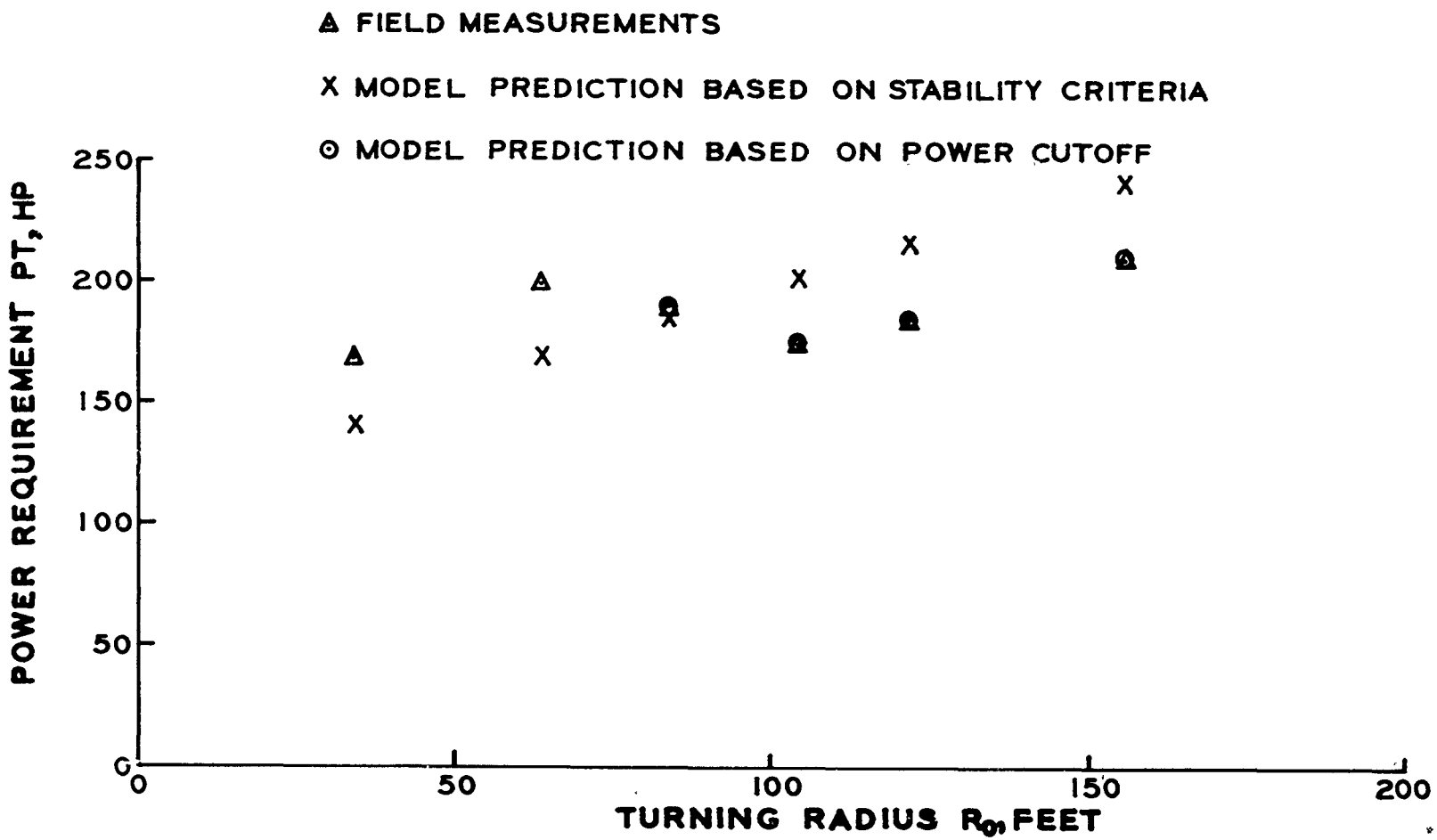

Figure 11. Power requirement versus turning radius for test series 107-111; comparison of model predictions with experimental data

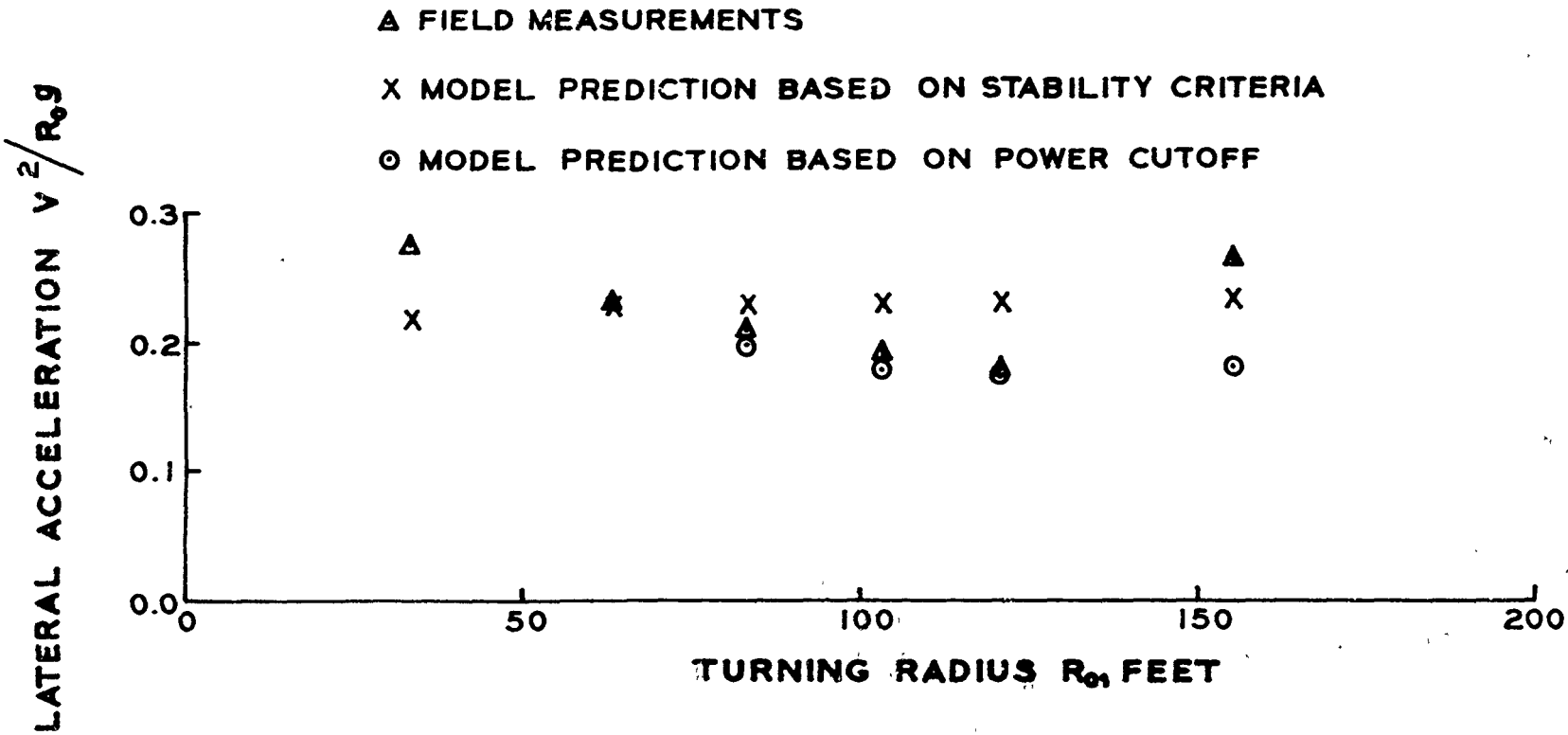

Figure 12. Lateral acceleration versus turning radius for test series 107-111; comparison of model predictions with experimental data

versus turning radius, vehicle speed versus turning radius, power requirement versus turning radius, and lateral acceleration versus turning radius, respectively. The model predictions in Figures 8 through 12 are based on both power cutoff and preliminary stability criteria. The turning radius-steering ratio relation shown in Figure 7, however, is unique for a given vehicle and soil condition. The power cutoff, as indicated, is controlled by the available power. According to Reference 7, the preliminary stability criteria are based on:

a. Rapid change in the slip velocity of the inner or the outer track.

b. The pivot point moves outside the front edge of the track-ground contact area (i.e., the offset equals 0.5 L when the center of gravity and center of geometry of the vehicle coincide).

c. Rapid decrease or increase in the turning radius.

These stability conditions usually take place at different vehicle velocities. The unstable vehicle velocity is chosen as the minimum of these velocities. For comparison with the experimental data the lower vehicle velocity corresponding to either the stability criteria or the power cutoff condition must be selected. As indicated in Figure 10, for the turning radii of 34 ft (test 111) and 64 ft (test 108) stability criteria control the velocity of the vehicle. For the turning radii of 83 ft (test 110), 104 ft and 121 ft (test 109), and 156 ft (test 107) the velocity of the vehicle is controlled by the available power. With this in mind, the experimental data in Figures 7 through 12 compare very favorably with the corresponding model predictions. This is particularly true in the case of track velocities and vehicle speed (Figures 8 through 10). Slight observable differences between the data and model predictions in Figures 7 through 12 should be expected because of the deviations in the test conditions from the steady-state mode of motion.

23. To demonstrate the ability of the terrain-vehicle model for treating transient motion, the response of the vehicle for test 107 was simulated for the entire test event. The measured time histories of the inner and outer track velocities were used to drive the model. For these specified driving conditions, the time histories of the vehicle speed, power requirements and lateral acceleration, and the trajectory of the center of gravity of the vehicle were then predicted and compared with the corresponding field measurements. Figure 13 depicts the time histories of the inner

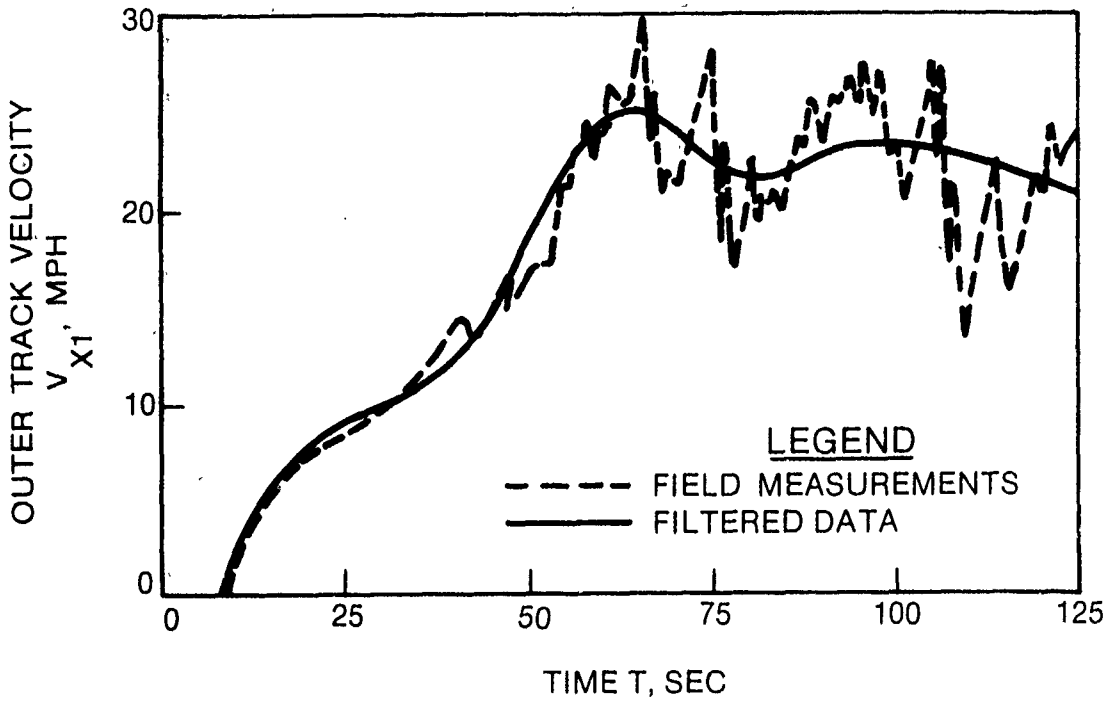

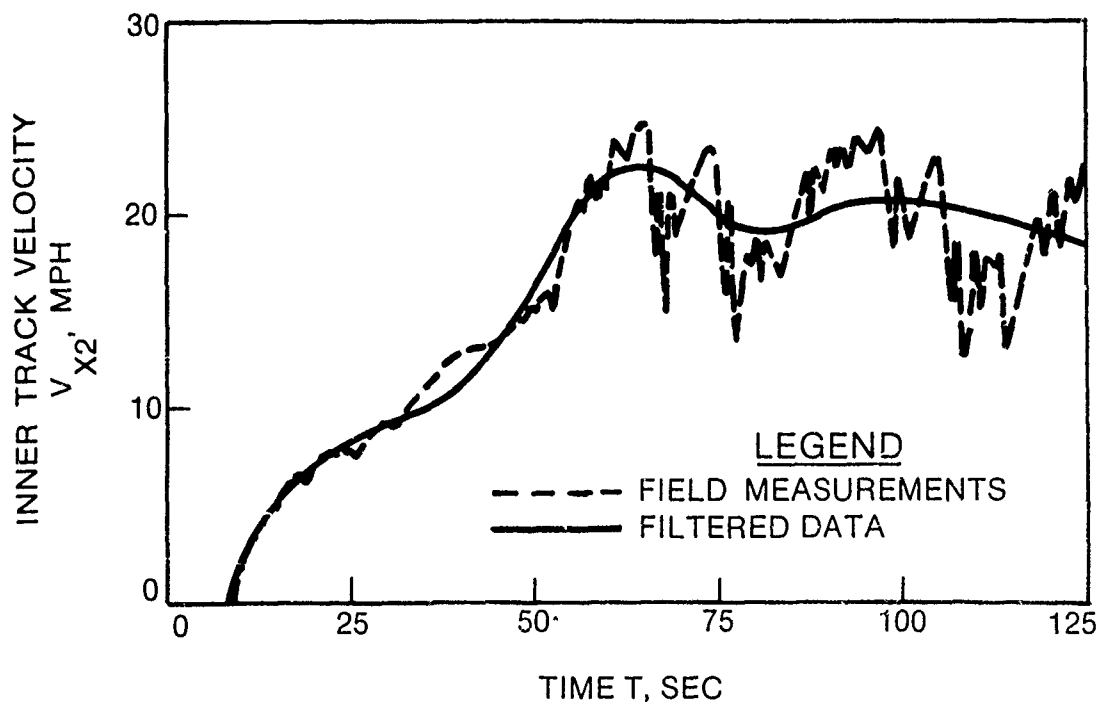

Figure 13. Outer and inner track velocity-time histories for test 107; field measurement and filtered data

and outer track velocities. The actual field measurements are quite noisy, particularly for times greater than approximately 60 sec. These high-frequency oscillations are believed to be mostly due to instrumentation and were filtered out. The filtered records are also shown in Figure 13 and are simply "best" fit curves to the field measurements satisfying the condition that the total area under both curves should be equal. These filtered track velocity-time histories were used as input to drive the terrain-vehicle model. Comparisons of the predicted time histories of the vehicle speed, power requirements, and lateral acceleration with the corresponding field measurements are shown in Figures 14 through 16, respectively. Similar to Figure 13, the field measurements are quite noisy. As anticipated, the predicted results do not manifest these oscillations because of the filtering of the input data. The degree of correlation of the predicted and measured results, however, is quite good, indicating that the modeling of the overall interaction between the terrain and the track is physically reasonable. Comparison of the predicted and measured trajectory of the center of gravity of the vehicle is shown in Figure 17. Again, the comparison between the predicted and measured results is quite favorable.

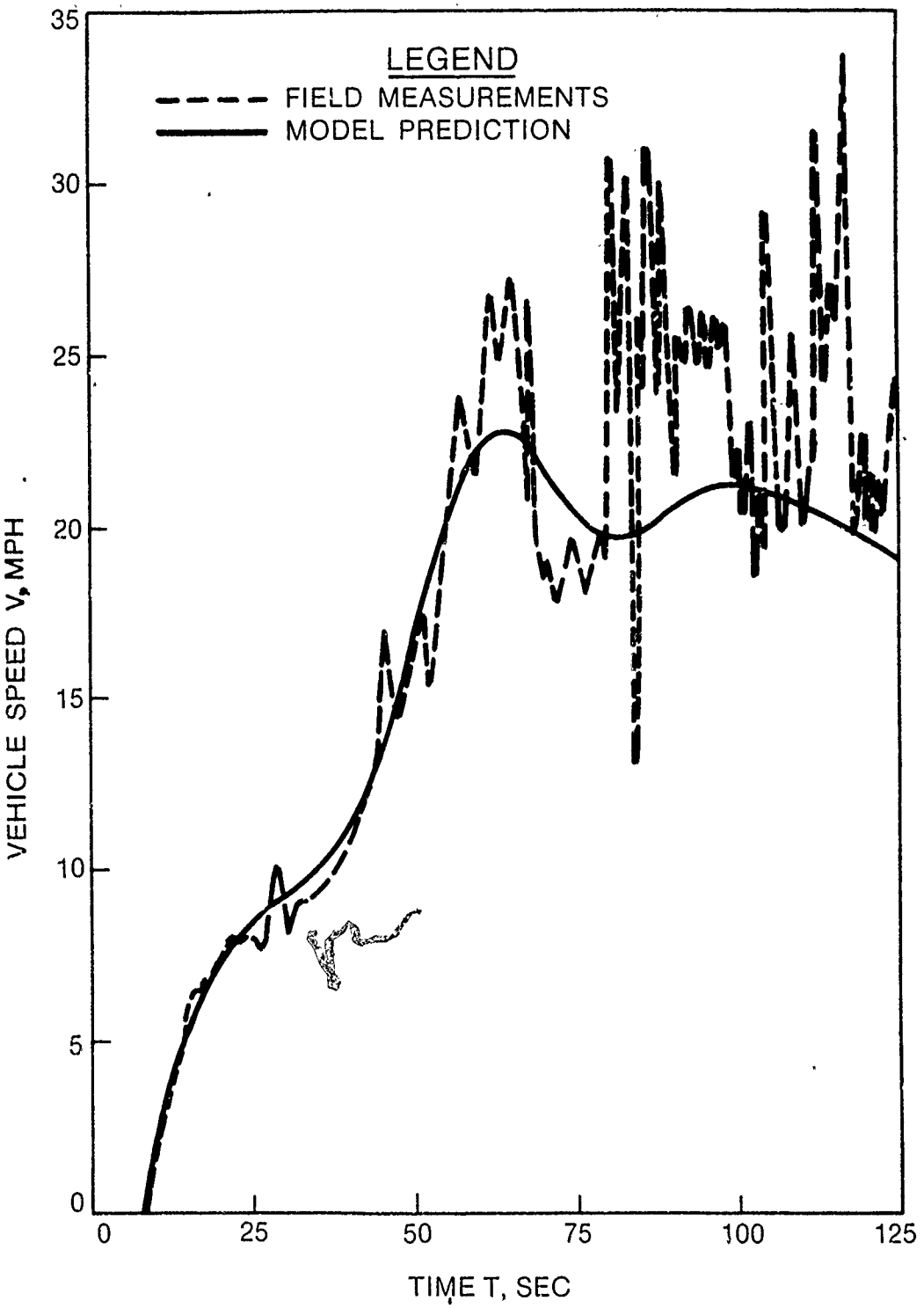

Figure 14. Vehicle speed-time history for test 107; comparison of model predictions with experimental data

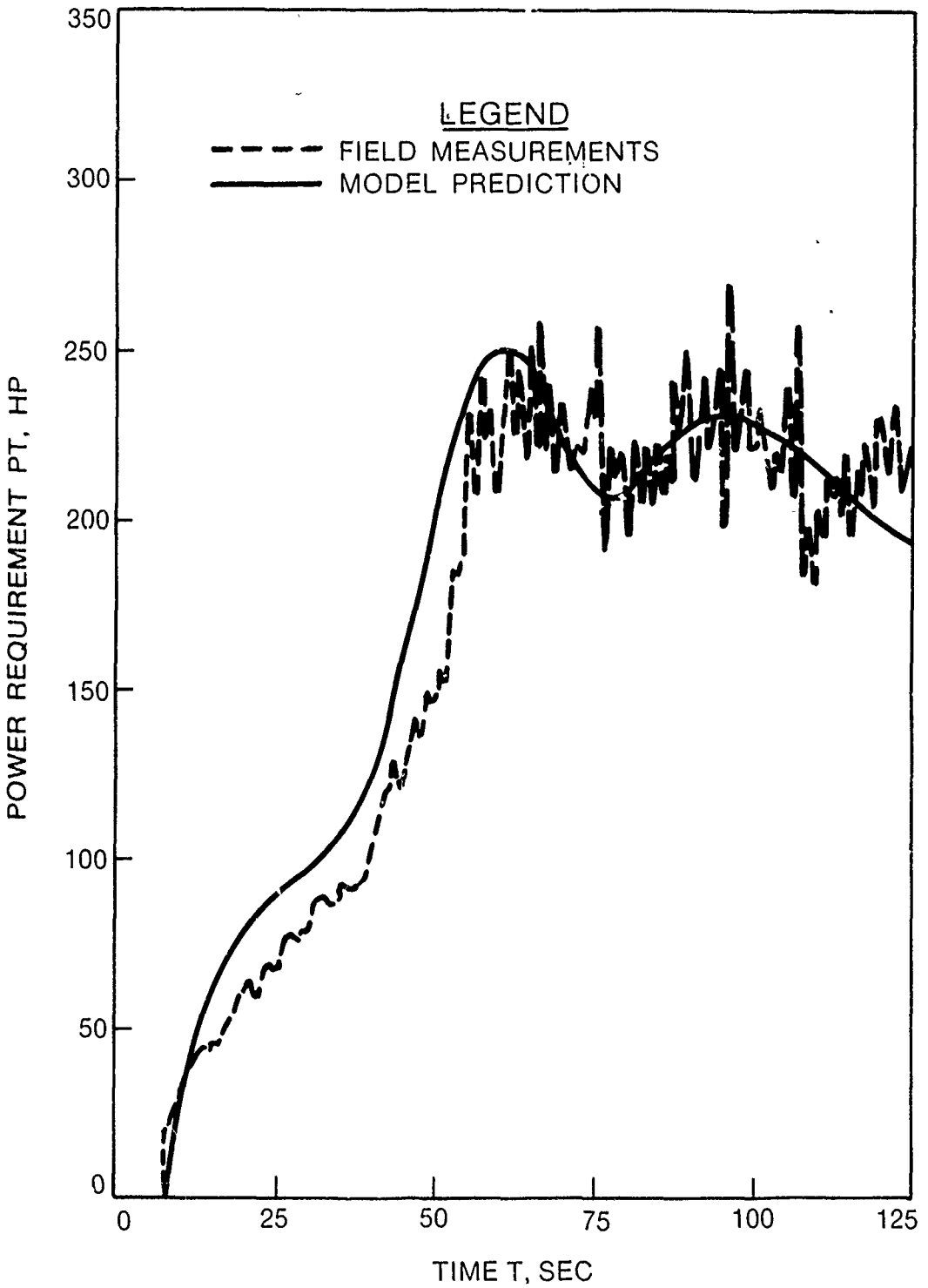

Figure 15. Total power-time history for test 107; comparison of model predictions with experimental data

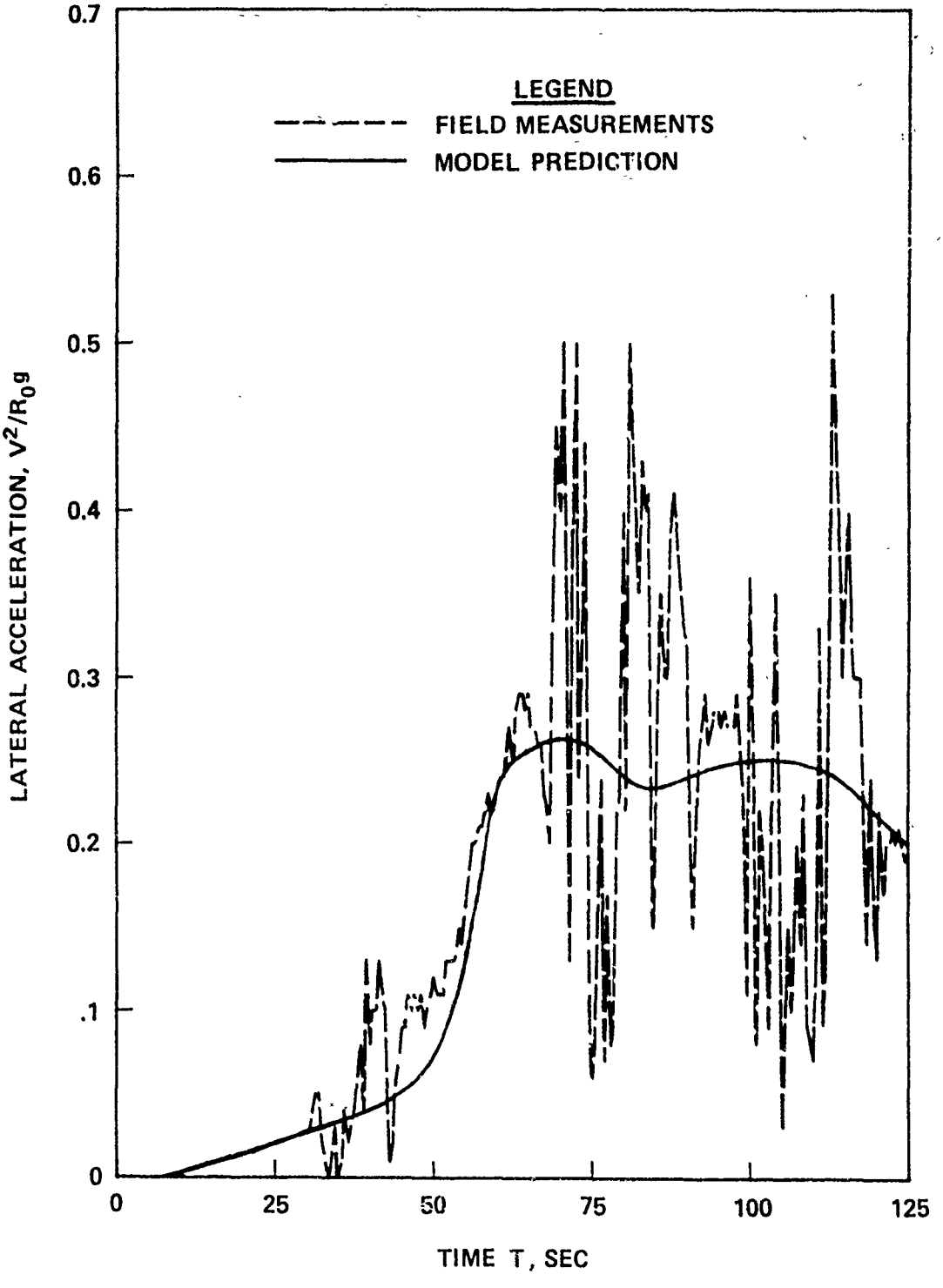

Figure 16. Lateral acceleration-time history for test 107; comparison of model predictions with experimental data

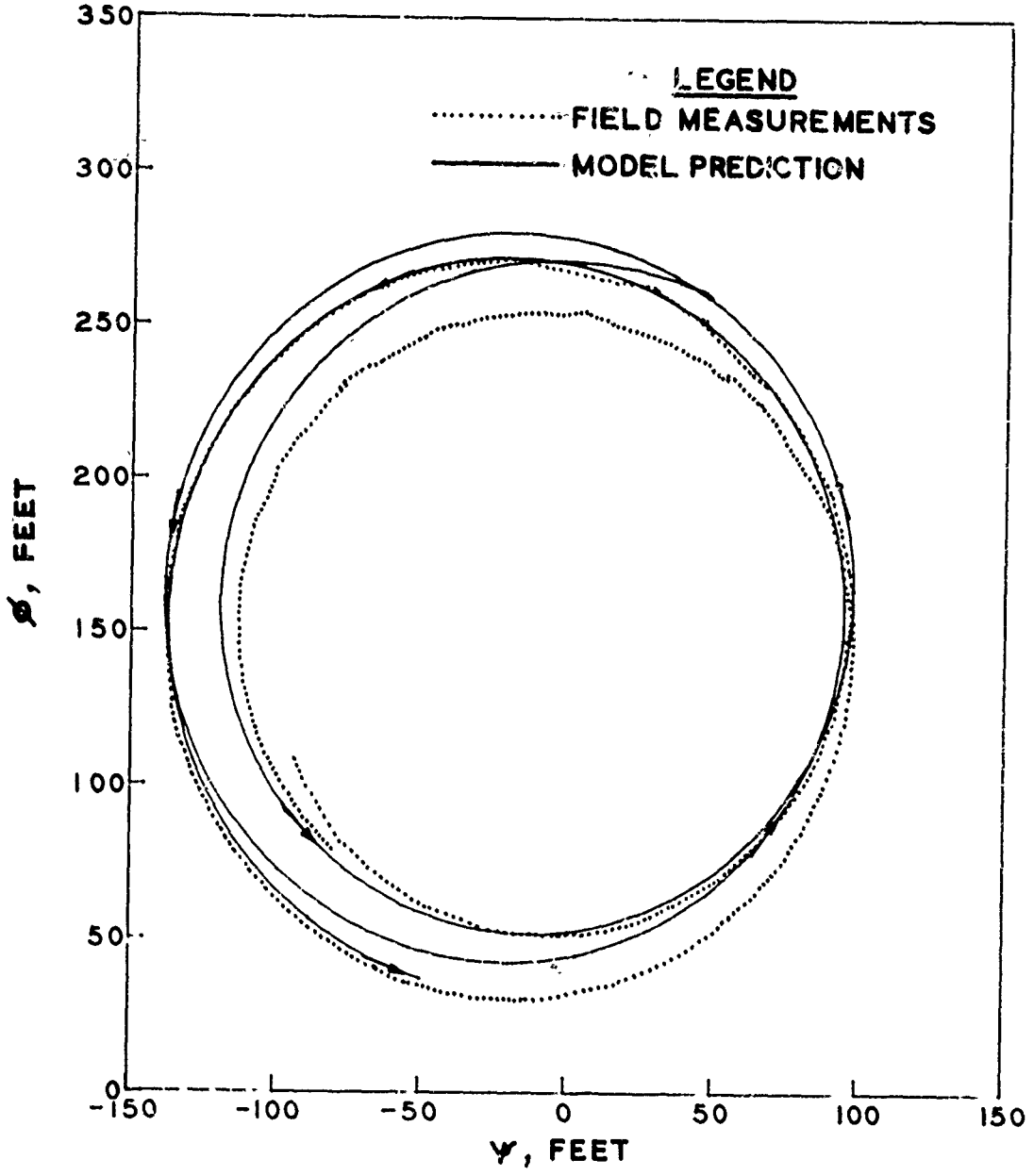

Figure 17. Trajectory of the center of gravity of the vehicle for test 107; comparison of model predictions with experimental data

PART V: SUMMARY AND CONCLUSION

24. A mathematical model of terrain-vehicle interaction for predicting the steering performance of track-laying vehicles has been developed and computerized for numerical application. The model contains some of the basic parameters governing the steering performance of tanks, such as track slippage, centrifugal forces, vehicle characteristics, and soil type. The model is applicable to both steady-state motion and transient motion under changing control commands. The model is partially validated by comparing field measurements for a specific vehicle with the corresponding model predictions. Efforts are presently under way at WES to compare the model predictions with experimental data for a broader range of test conditions.

REFERENCES

1. Bekker, M. B.; The Theory of Land Locomotion; 1963; The University of Michigan Press, Ann Arbor, MI.

2. Hayashi, I.; "Practical Analysis of Tracked Vehicle Steering Depending on Longitudinal Track Slippage," Proceedings, The International Society for Terrain Vehicle Systems Conference, Vol 2; 1963; p 493.

3. Kitano, M. and Jyorzaki, H.; "A Theoretical Analysis of Steerability of Tracked Vehicles," Journal of Terramechanics, The International Society for Terrain Vehicle Systems, Vol 13, No. 4; 1976; pp 241-258.

4. Kitano, M. and Kuma, M.; "An Analysis of Horizontal Plane Motion of Tracked Vehicles," Journal of Terramechanics, The International Society for Terrain Vehicle Systems, Vol 14, No. 4; 1977; pp 221-225.

5. Baladi, G. Y. and Rohani, B.; "A Mathematical Model of Terrain-Vehicle Interaction for Predicting the Steering Performance of Track-Laying Vehicles," Proceedings of the 6th International Conference of the International Society for Terrain-Vehicle Systems; 1978; Vienna, Austria.

6. Kondner, R. L.; "Hyperbolic Stress-strain Response: Cohesive Soils," Journal, Soil Mechanics and Foundations Division, American Society of Civil Engineers, Vol 89, No. SM1; Feb 1963; pp 115-143.

7. Baladi, G. Y. and Rohani, B.; "A Terrain-Vehicle Interaction Model for Analysis of Steering Performance of Track-Laying Vehicles"; Technical Report GL-79-6, 1979; U. S. Army Engineer Waterways Experiment Station, CE, Vicksburg, MS.

8. Rula, A. A. and Nuttall, C. J., Jr.; "An Analysis of Ground Mobility Models (ANAMOB)"; Technical Report M-71-4, July 1971; U. S. Army Engineer Waterways Experiment Station, CE, Vicksburg, MS.

9. Waterways Experiment Station: "The Unified Soil Classification System"; Technical Memorandum No. 3-357, 1953; Office of the Chief of Engineers, U. S. Army.

APPENDIX A

NOTATION

a	AL^2/W
A	Soil parameter
b	B/L
B	Track tread
c	CL^2/W
c_d	C_dL^2/W
c_X	C_X/L
C	Static cohesive component of shear strength
C_d	Added cohesive strength due to dynamic loading
C_X	Abscissa of the center of gravity of the vehicle
C_1	Slip radius of the outer track
C_2	Slip radius of the inner track
CG	Center of gravity of the vehicle
CI	WES cone index
CR	Center of rotation of the vehicle
d	D/L
D	Track width
f_{CX}	F_{CX}/W
f_{CY}	F_{CY}/W
F_C	Inertial force
F_{CX}	Longitudinal component of inertial force
F_{CY}	Transverse component of inertial force
δ	Coefficient of rolling resistance
g	Acceleration due to gravity
G	Initial shear stiffness coefficient
h	H/L
H	Height of center of gravity
I_z	Mass moment of inertia of the vehicle about an axis passing through its center of gravity and parallel to the Z axis
IC_1	Center of slip rotation of the outer track

IC_2	Center of slip rotation of the inner track
ICR	Instantaneous center of rotation of the vehicle
L	Contact length of track
m	ML^2/W
M	Soil parameter
n	NW/L^2
N	Soil parameter
O	Center of geometry of the vehicle
p	P/L
P	Offset (distance from center of gravity to pivot point of vehicle)
PT	Total power = PT1 + PT2
PT1	Power required by the sprocket of the outer track
PT2	Power required by the sprocket of the inner track
PTD	Differential power = PT1 - PT2
$q_1(x)$	$dL^2Q_1(x)/W$
$q_2(x)$	$dL^2Q_2(x)/W$
$Q_1(X)$	Transverse component of shear stress along the outer track
$Q_2(X)$	Transverse component of shear stress along the inner track
$r_1(x)$	$dL^2R_1(x)/W$
$r_2(x)$	$dL^2R_2(x)/W$
$\tilde{R}$	Ordinate of the instantaneous center of rotation of the vehicle
R_o	Radius of the trajectory of the center of gravity of the vehicle
R_s	Rolling resistance
$R_1(X)$	Normal stress under the outer track
$R_2(X)$	Normal stress under the inner track
R_I	Instantaneous radius of curvature
t	Time
$t_1(x)$	$dL^2T_1(x)/W$
$t_2(x)$	$dL^2T_2(x)/W$

$T_1(X)$	Longitudinal component of shear stress along the outer track
$T_2(X)$	Longitudinal component of shear stress along the inner track
v	Velocity of the vehicle
v_{s1}	Total slip velocity of the outer track
v_{s2}	Total slip velocity of the inner track
v_{sX1}	Longitudinal component of slip velocity of the outer track
v_{sX2}	Longitudinal component of slip velocity of the inner track
v_{sY1}	Transverse component of slip velocity of the outer track
v_{sY2}	Transverse component of slip velocity of the inner track
v_X	Longitudinal component of velocity of the vehicle
v_{X1}	Longitudinal component of velocity of the outer track
v_{X2}	Longitudinal component of velocity of the inner track
v_Y	Transverse component of velocity of the vehicle
W	Weight of the vehicle
x	X/L
X,Y,Z	Local coordinate system
y	Y/L
z	Z/L
α	Side-slip angle
γ_1	Angle of slip direction of the outer track
γ_2	Angle of slip direction of the inner track
Δ	Shearing deformation
Δ_{I1}	Initial displacement of the outer track
Δ_{I2}	Initial displacement of the inner track
Δ_1	Shearing deformation of soil under the outer track
$\dot{\Delta}_1$	Time rate of shearing deformation
Δ_2	Shearing deformation of soil under the inner track
$\dot{\Delta}_2$	Time rate of shearing deformation

δ_1	Δ_1/L
$\dot{\delta}_1$	$\dot{\Delta}_1/L$
δ_2	Δ_2/L
$\dot{\delta}_2$	$\dot{\Delta}_2/L$
ε	Steering ratio
θ	Directional angle
Λ	Material constant related to rate effect
λ	ΛL
μ	GL^3/W
ξ_1	C_1/L
ξ_2	C_2/L
σ	Normal stress
τ	Shear stress
τ_M	Maximum shear strength
ψ, Φ	Coordinate system fixed on level ground
ω	Yaw angle

In accordance with letter from DAEN-RDC, DAEN-ASI dated 22 July 1977, Subject: Facsimile Catalog Cards for Laboratory Technical Publications, a facsimile catalog card in Library of Congress MARC format is reproduced below.

Baladi, George Y.
Analysis of steerability of tracked vehicles; theoretical predictions versus field measurements : Final report / by George Y. Baladi, Behzad Rohani (Structures Laboratory, U.S. Army Engineer Waterways Experiment Station) ; prepared for Office, Chief of Engineers, U.S. Army ; monitored by Geotechnical Laboratory, U.S. Army Engineer Waterways Experiment Station ; Springfield, Va. : available from NTIS, 1981.
39, 4 p. : ill. ; 27 cm. -- (Miscellaneous paper / U.S. Army Engineer Waterways Experiment Station ; SL-81-3)
Cover title.
"March 1981."
"Under Project 4A161102AT22 Task CO, Work Unit 001."
Bibliography: p. 39.

1. AGIL (Computer program). 2. Computer programs. 3. Mathematical models. 4. Soil mechanics. 5. Track-laying vehicles. 6. Vehicles, Military. I. Rohani, Behzad. II. United States. Army. Corps of Engineers.

Baladi, George Y.
Analysis of steerability of tracked vehicles : ... 1981.

Office of the Chief of Engineers. III. United States. Army Engineer Waterways Experiment Station. Structures Laboratory. IV. Title V. Series: Miscellaneous paper (United States. Army Engineer Waterways Experiment Station) ; SL-81-3.
TA7.W34m no.SL-81-3